



HIGHLIGHTED PAPER



Highly stretchable self-sensing actuator based on conductive photothermally-responsive hydrogel

Chiao-Yueh Lo^{1,†}, Yusen Zhao^{1,†}, Cheolgyu Kim^{1,†}, Yousif Alsaied¹, Roozbeh Khodambashi², Matthew Peet³, Rebecca Fisher^{4,5}, Hamid Marvi⁶, Spring Berman⁶, Daniel Aukes², Ximin He^{1,*}

¹ Department of Material Science and Engineering, University of California Los Angeles, Los Angeles, CA 90095, USA

² The Polytechnic School, Ira A. Fulton Schools of Engineering, Arizona State University, Mesa, AZ 85212, USA

³ Department of Mechanical and Aerospace Engineering, Arizona State University, Tempe, AZ 85287, USA

⁴ School of Life Science, Arizona State University, Tempe, AZ 85287, USA

⁵ Department of Basic Medical Sciences, University of Arizona College of Medicine-Phoenix, Phoenix, AZ 85004, USA

⁶ School for Engineering of Matter, Transport and Energy, Arizona State University, Tempe, AZ 85287, USA

Soft robots built with active soft materials have been increasingly attractive. Despite tremendous efforts in soft sensors and actuators, it remains extremely challenging to construct intelligent soft materials that simultaneously actuate and sense their own motions, resembling living organisms' neuromuscular behaviors. This work presents a soft robotic strategy that couples actuation and strain-sensing into a single homogeneous material, composed of an interpenetrating double-network of a nanostructured thermo-responsive hydrogel poly(N-isopropylacrylamide) (PNIPAAm) and a light-absorbing, electrically conductive polymer polypyrrole (PPy). This design grants the material both photo/thermal-responsiveness and piezoresistive-responsiveness, enabling remotely-triggered actuation and local strain-sensing. This self-sensing actuating soft material demonstrated ultra-high stretchability (210%) and large volume shrinkage (70%) rapidly upon irradiation or heating (13%/°C, 6-time faster than conventional PNIPAAm). The significant deswelling of the hydrogel network induces densification of percolation in the PPy network, leading to a drastic conductivity change upon locomotion with a gauge factor of 1.0. The material demonstrated a variety of precise and remotely-driven photo-responsive locomotion such as signal-tracking, bending, weightlifting, object grasping and transporting, while simultaneously monitoring these motions itself via real-time resistance change. The multifunctional sensory actuatable materials may lead to the next-generation soft robots of higher levels of autonomy and complexity with self-diagnostic feedback control.

Keywords: Photothermal responsive hydrogel; Conducting polymer; LCST; Strain sensor; Self-monitoring; Soft actuator; Soft robotics

Introduction

Living organisms can sense external stimuli (exteroception) and their own movement (proprioception) while moving automatically in response to the environment, attributed to their somatosensory and neuromuscular systems. Specifically, human

* Corresponding author.

E-mail address: He, X. (ximinhe@ucla.edu)

† These authors contributed equally.

fingers and other entirely soft animal structures (e.g. octopus arms and elephant trunks) can perform complex tasks with serial movements. In contrast, man-made robots are conventionally rigid and accomplish sensory motion tasks by coupling sensors, external cameras, and actuators with computational control systems; these coupled systems enable motion-monitoring to provide feedback on locomotive gaits and terrain conditions [1]. For typical robots, achieving actuation with closed-loop control requires mounting sensing devices, such as encoders, accelerometers, triboelectric nanogenerators, or linear variable differential transformers. These complex multi-electronics integrations restrict the size miniaturization and higher-level motility [2].

Soft robots made of compliant materials can conform to their surroundings through continuous and dexterous maneuvers. Despite tremendous efforts, realizing intelligent soft actuators with self-sensing capabilities remains a challenge. Specifically, current state-of-the-art actuation strategies such as asymmetric expansion [3–4], pneumatic inflation [5], and hydraulic actuation [6] usually utilize materials that serve purely structural purposes and cannot themselves be stimulated by trigger signals; thus, they are unable to sense their own motions. To achieve self-sensing function in actuators, roboticists have physically laminated or embedded various sensing devices based on optical loss [7–9], capacitance [10], electroluminescence [10], triboelectricity [11], and piezoresistivity [3,10,12–18]. However, device damage at the interface can arise from modulus mismatch between the sensor and actuator [19]. The sensing and actuation modules are also predefined, restricting deformation when dealing with a complicated and ever-changing environment.

To mimic the large deformation, fast environmental response, and multifunctional motion of living creatures, people have developed actuators made from new stimuli-responsive polymers such as liquid crystalline elastomers (LCEs) [20], electroactive polymers (EAPs) [21], shape memory polymers (SMPs) [22], and stimuli-responsive hydrogels [23]. These materials are intrinsically stimuli-responsive and are thus capable of realizing local deformation with high dexterity and complexity. Among these soft responsive polymers, hydrogels carry the potential to achieve multi-functionality due to their ability to experience significant volumetric change in response to a variety of environmental stimuli such as temperature [24–25], light [26], pH [27–28], electric field [29], and chemicals [30]. Their unique and attractive abilities as actuators have led to multifarious applications in soft robotics at various length scales ranging from micro-robots for drug delivery [31–32] to macro actuators for object manipulation [33–34]. Additionally, serving as sensors, hydrogels can withstand ultra-high tensile strains [35].

Stretchable polymeric matrices embedded with conductive fillers have been widely used as strain sensors due to their ultra-high stretchability, direct current (DC) compatibility, facile fabrication, and tunable deformation-dependence of resistivity achieved via changing the percolation of the conductive filler network. Carbon black [36], carbon nanotubes [37], graphene derivatives [38], and liquid metals [18] have been reported as effective conductive fillers, and their sensing range can reach up to 400% strain [39]. However, the immiscible filler particles in the composite naturally tend to aggregate during fabrication, hindering the adaptive movements and causing irreversible

device damage [40]. Conducting polymers (CPs) offer promising alternatives as conductive and piezo-resistivity fillers due to their neuron-like electrical conductivity [41–43]. As a matter of fact, CPs are typically stiff and lack stretchability due to their huge, planar electron conjugating system and rigid molecular chains. One route to address the issues of elasticity and flexibility in both sensing and actuation systems is to homogeneously incorporate interconnected CPs in soft, flexible matrices.

By molecularly integrating the stimuli-responsive hydrogels and CPs, the actuation and sensing can be achieved simultaneously. Although CP-percolated hydrogels have been reported [44], self-sensing actuation remains unachieved because of the following issues: (a) hydrogels are typically weak and CPs are brittle, leading to low flexibility and stretchability; (b) diffusion of CPs into hydrogel network is slow using conventional solution-based fabrication techniques, resulting in a percolation only on the hydrogel skin [45]; (c) actuation performance is usually diffusion-limited, with a slow response time of minutes to hours [46]. Hence, creating a CP-percolated stimuli-responsive hydrogel with high stretchability, high homogeneity, fast response, and capability for deformation sensing (proprioceptive and exteroceptive) is highly desired.

Herein, we have demonstrated a two-in-one functional hydrogel that couples independent actuation and strain-sensing capabilities from the photo-thermal-mechanical pathway and piezoresistive mechanism, respectively. The homogeneous CP-percolated double-network hydrogel was constructed by combining thermal-responsive, soft, and elastic poly(*N*-isopropylacrylamide) (PNIPAAm), the actuator component, with black conducting polymer polypyrrole (PPy), the light absorbing and piezoresistive component. The nano-structured PNIPAAm hydrogel enabled high stretchability (>210%), high response rate (6-fold faster than conventional PNIPAAm) and substantial volume change ($\Delta V/V = 70\%$) in water. The PPy network was incorporated into the PNIPAAm with a modified solution method, which not only effectively prohibited delamination and filler aggregation, but also provided uniform PPy distribution for samples up to 3 mm in thickness. We fabricated a compositionally and geometrically homogeneous cylindrical pillar as a light-responsive actuator, capable of rapidly and omni-directionally self-orienting towards incident near-infrared (NIR) light, resembling living plants' phototropic behavior. Meanwhile, the piezoresistive sensing behavior was observed up to >200% tensile strain and with a gauge factor (GF, $\Delta R/R_0/\epsilon$) of 1.0, which is within the typical range for high-strain soft sensors [47]. Furthermore, the self-sensing actuation abilities have been demonstrated by photo-induced tracking, bending, weightlifting, grasping and object moving with real-time sensing via resistance change. With its demonstrated high sensitivity and actuation strain, this conductive self-sensing hydrogel can lay the foundation for unconventional soft robots with a self-diagnostic feedback-controlled higher level of autonomy.

Results and discussion

To build a composite hydrogel actuator with self-sensing ability, we chose to combine PNIPAAm and PPy into a double-network as an exemplary material. PNIPAAm provides both

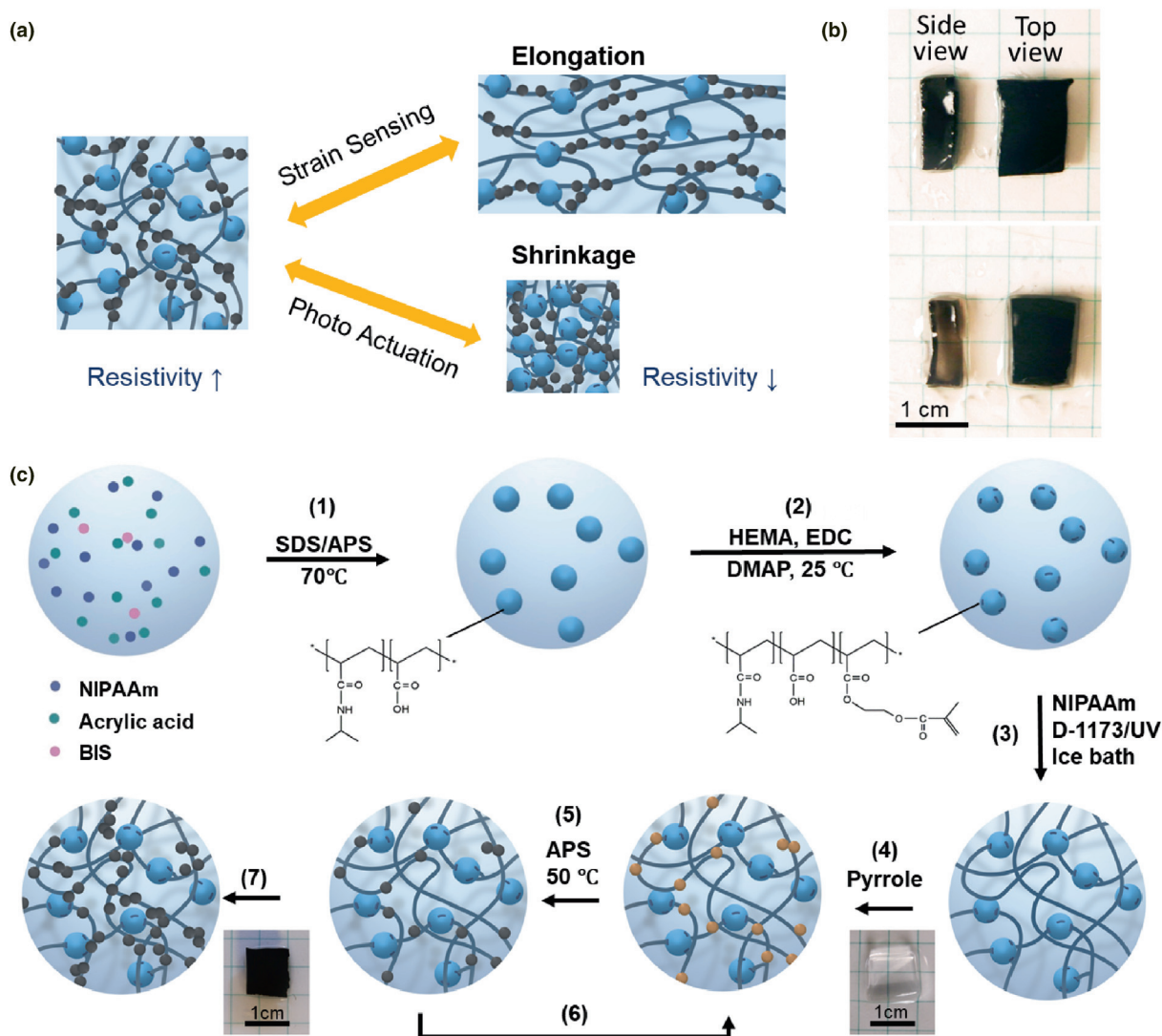


FIGURE 1

(a) Schematic of mechanism of the self-sensing actuator: Resistivity change of conducting polymer network when exposed to external stress or thermal stimulated volumetric change. (b) Comparison of the conventional synthesis method with poor PPy distribution in the PNIPAAm hydrogel (bottom) with the modified method for homogeneous PPy loading throughout the network (top) (c) Fabrication procedure of P(NIPAAm-co-AA) nanogels and c-NanoH.

thermo-responsive actuation and mechanical flexibility, while PPy acts as a photothermal transducer, piezoresistive sensor, and mechanical strengthener. Under light illumination, the optical energy is absorbed by PPy and converted into thermal energy, resulting in temperature increase of the material. When temperature increases over the lower critical solution temperature (LCST) of PNIPAAm, the resistivity of the hydrogel is significantly reduced as the PPy network becomes more compacted upon temperature-driven shrinkage of the PNIPAAm network (Fig. 1a) [48,49].

First, the PNIPAAm network was synthesized. To achieve large volume change under repeated shrinking and swelling, we molecularly synthesized and incorporated 2-hydroxyethyl methacrylate (HEMA)-functionalized poly(NIPAAm-co-AA) nanostructured hydrogel beads (nanogel) into the composite network as crosslinking sites. Particularly, HEMA is esterized with PAA blocks to provide non-reacted double bonds, which is used as bonding sites

during crosslinking. Compared to traditional crosslinkers such as *N,N'*-methylenebis(acrylamide) (BIS), the nanogel crosslinker results in higher elasticity, faster thermal-responsive volume change, and larger volume change under deswelling.

Special considerations must be taken when introducing PPy into the as-prepared PNIPAAm hydrogel network. Conventionally, the diffusion of PPy into hydrogels is limited by PPy's relatively large and hydrophobic particle sizes [50] that are difficult to infiltrate into the hydrogel's nanomesh pores [45,51,52]. In addition, the highly exothermic PPy reaction unavoidably increases the local temperature above PNIPAAm's LCST, resulting in the local shrinkage of PNIPAAm that further hinders the diffusion of pyrrole monomers [53]. This process typically results in an inhomogeneous material with a conducting polymer-rich shell and non-conductive core (Fig. 1b). To solve the issue, we replaced the aqueous prepolymer solution with a DMSO solution, in which PNIPAAm exhibits an upper critical solution

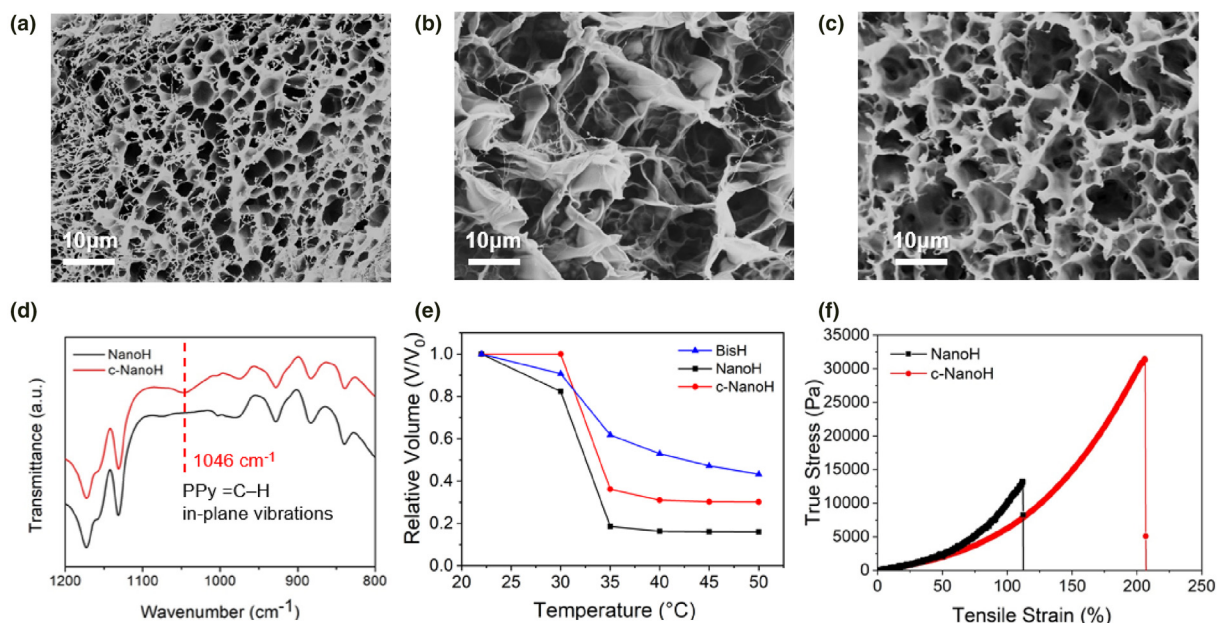


FIGURE 2

SEM images of (a) conventional BIS-crosslinked PNIPAAm hydrogel (BisH), exhibiting relatively small pores, (b) nanogel-crosslinked PNIPAAm hydrogel (NanoH with large pore crosslinked by nanogel), and (c) c-NanoH after PPy incorporation. Larger porous structure with nanogel enabled faster water exchange and phase transition. (d) FTIR spectrum of NanoH before and after PPy incorporation: PPy peak at 1046 cm⁻¹ confirmed PPy in c-NanoH. (e) Equilibrium deswelling ratio of BisH, NanoH, and c-NanoH from 20 °C to 50 °C. (f) Tensile stress–strain curves of nano-structured hydrogels showing enhanced elongation and fracture strength after coating with PPy.

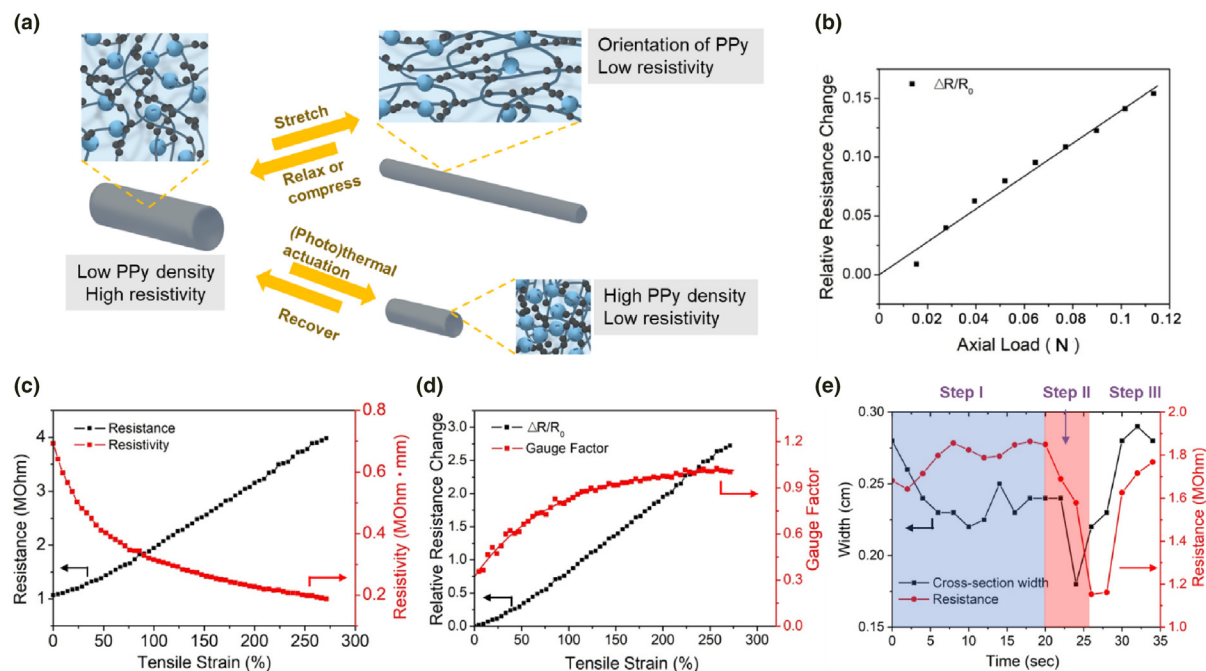


FIGURE 3

(a) Resistivity changes with stretching, compression, and (photo)thermal actuation due to change in alignment and apparent density of the conducting PPy network. (b) Resistance change as a function of axial load at small compression deformation (axial stress < 1 kPa), showing linear behavior. (c) Resistivity and resistance change as a function of tensile strain, showing that for large tensile stretch, resistivity decreases with strain. The mechanism can be described in (a). (d) Strain sensing performance of c-NanoH, demonstrating ultra-high strain sensing range (up to 280%) with decent sensitivity at high strain (GF = 1). (e) Resistance measurement on c-NanoH with fixed length. In the blue region, the resistance increased possibly due to isolation during the PNIPAAm phase transition. In the red region, the resistance abruptly decreased due to the density change of the PPy network.

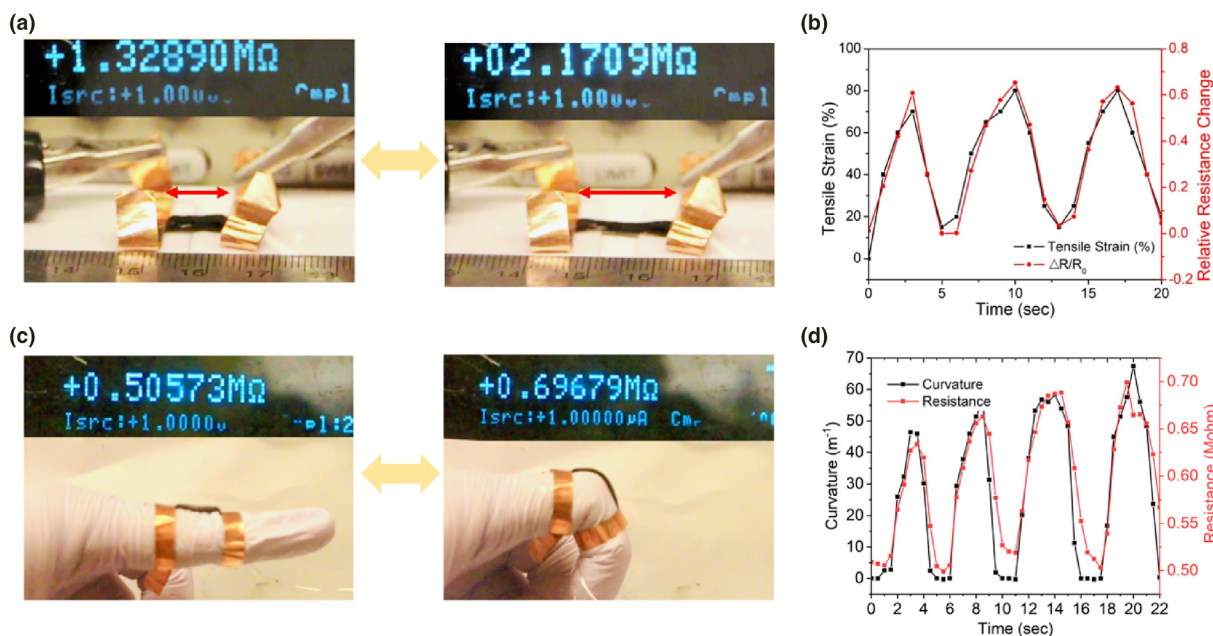


FIGURE 4

(a), (b) Demonstration of stable real-time cyclic stretch strain sensing, and (c), (d) real-time curvature sensing on a human forefinger.

temperature (UCST) behavior and does not shrink upon heating [54]. The kinetics of polymerization is also greatly reduced, enabling the complete mixing of pyrrole with the oxidant prior to polymerization, otherwise impossible with a very fast reaction. Consequently, a much more uniform PNIPAAm/conducting polymer hybrid material was obtained (Fig. 1b).

Characterized by scanning electron microscopy (SEM), the nano-structured hydrogel without PPy (termed NanoH) presented a hierarchical porous structure (Fig. 2b). The pore size was significantly larger than the control hydrogel crosslinked with BIS (termed BisH) (Fig. 2a). After incorporating NanoH with PPy, the hydrogel (termed c-NanoH) exhibited similar pore size and morphology to NanoH (Fig. 2c). Such relatively large pores provided paths of effective water diffusion, leading to the high response and recovery speeds of c-NanoH, in contrast to the BisH. To further confirm the successful PPy incorporation, we utilized FT-IR spectroscopy. The PPy-incorporated c-NanoH exhibited a specific peak at 1046 cm^{-1} , ascribed to the =C–H in-plane vibration of PPy (Fig. 2d). In comparison, NanoH without PPy did not show this specific peak.

To examine the deformation capability of the nanostructured hydrogels, we analyzed the temperature-dependent hydrogel shrinkage of c-NanoH, NanoH, and BisH after 15 min immersion in water of different temperatures. As shown in Fig. 2e, both NanoH and c-NanoH achieved large phase transition when heated to near the LCST ($30\text{ }^{\circ}\text{C}$ – $35\text{ }^{\circ}\text{C}$), demonstrating a remarkable equilibrium volume change of $13\%/^{\circ}\text{C}$, substantially higher than that of BisH ($6\%/^{\circ}\text{C}$). Note that the overall volume changes of both c-NanoH and NanoH were also significantly larger (70% and 84% shrinkage, respectively) than BisH (57% shrinkage). This enhanced deswelling performance possibly arose from the nano-sized crosslinking sites as well as the loosely crosslinked,

flexible PNIPAAm chains grafting onto the nanogel [55]. Upon immersion in water at elevated temperatures, the flexible PNIPAAm chains can freely aggregate with the nanogel, leaving sufficient space for water to diffuse out of the network. The slightly decreased shrinkage of c-NanoH compared to NanoH can be attributed to the stiff and non-thermal-responsive PPy network, but the overall c-NanoH network was still more thermal-responsive than BisH. To further evaluate the thermal response rate, the three hydrogels were cut into $1.0\text{ cm} \times 1.0\text{ cm} \times 0.4\text{ cm}$ samples and swollen sufficiently in water at $25\text{ }^{\circ}\text{C}$ followed by immersion in a hot water tank. The hydrogel volumes were recorded gradually with time, and the volumetric change rates were compared (Fig. S1). The initial volumetric shrinkage rates of NanoH (16.6%) and c-NanoH (23.6%) within the first 30 s were significantly faster than that of BisH (4.0%). This result was consistent with the larger pore sizes demonstrated by SEM images in Fig. 2 (a)–(c).

We utilized stress–strain curves from uniaxial stretching to characterize and describe the mechanical properties of the composite hydrogel. The fracture stress of the composite hydrogel after introducing a PPy network (c-NanoH) increased to 30 kPa , compared to 13 kPa for NanoH. Interestingly, c-NanoH also demonstrated an enhanced fracture strain of 210% , compared to 115% for NanoH (Fig. 2f). Although pure PPy is rigid and lacks elasticity, we speculate that this enhanced elastic behavior can be attributed to the interpenetration of PPy and NanoH networks. Because the PNIPAAm polymer chains are more entangled in DMSO while in-situ polymerizing PPy, the PNIPAAm polymeric chains are confined by PPy in the coil state. This higher degree of entanglement of polymeric chains and the nanostructure in the c-NanoH hydrogels resulted in improved elastic properties and stretchability [55].

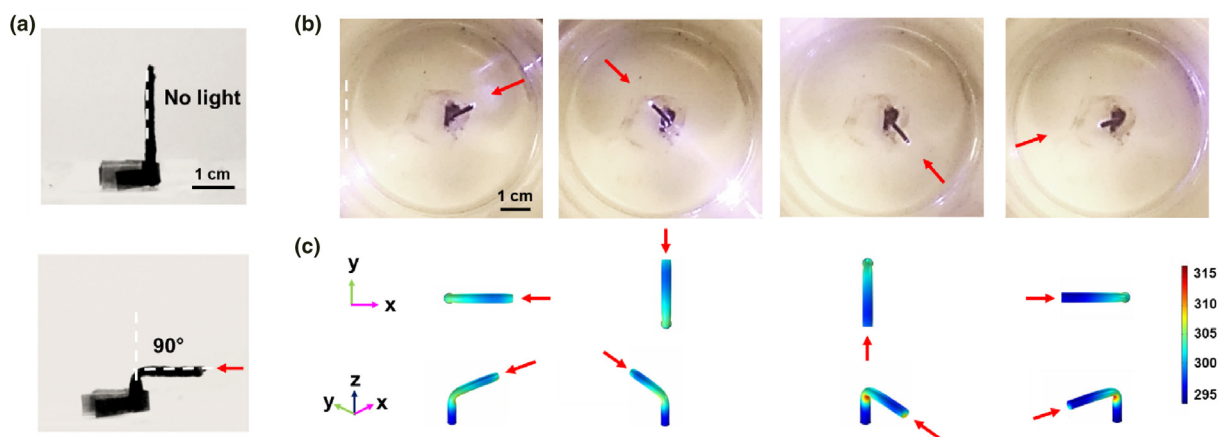


FIGURE 5

(a) Side view of a (top) c-NanoH pillar standing upright and (bottom) light-induced pillar bending to 90°. (b) Top view of omnidirectional light tracking from 4 different directions, showing versatile actuation in response to the direction of light source. (c) Simulation results of shape deformation and temperature gradient on omnidirectional tracking pillar. Light from four different azimuthal angles were applied on the pillar and the color indicates the temperature distribution. The unit of the color code is Kelvin.

To realize self-sensing capability, we utilized a resistivity change mechanism of c-NanoH upon stretching. The sensing measurement was conducted by connecting the c-NanoH hydrogel in a circuit. As depicted in Fig. 3a, the resistance change of c-NanoH under external strain or stimulated actuation can be attributed to two factors: (1) the structural effect, involving passive elongation along the tensile direction and Poisson contraction along the lateral direction. For a conducting polymer hydrogel, the resistance ratio follows $R/R_0 < \lambda^2$ due to the reorientation and alignment of coiled conducting polymer along the tensile direction, where R/R_0 is the normalized resistance under strain and λ is the axial stretch ratio [56]; (2) the density effect: in the stimuli-induced shrinkage of a hydrogel network, PPy density is increased, and microstructure transits from a loosely compact, disconnected network to a highly compact, connected network. Such a highly compact state facilitates the overlap between delocalized π -orbitals and a higher probability for electrons to migrate via intra-chain migration and inter-chain hopping [44].

Under external stretching or compression, the PPy chains are stretched or contracted to modulate the resistance. Notably, we observed a structural effect under very small compression deformation (axial stress < 1 kPa), as shown in Fig. 3b (Video S1). The resistance change can also be approximated as linear fashion. With respect to tensile stretching, the resistance continued to increase with strain. The resistivity calculated according to the dimensional change decreased at larger tensile strains (Fig. 3c). This might be attributed to the chain alignment of PPy chains along stretching direction [57]. In Fig. 3d, the calculated gauge factor (*i.e.*, the slope of $\Delta R/R$ vs. strain) increased with strain and reached a maximum value of 1.0 at the fracture point.

During passive mechanical deformation under external force, the hydrogel composite experiences no volume change. However, under (photo)thermal response, the volume actively shrinks locally at the response site. To monitor the resistance change under its active deformation, we fixed the hydrogel at

two terminals to restrict axial contraction and illuminated NIR light to induce photothermal shrinkage (Fig. 3e). The resistance was measured in real-time along the axial direction. Interestingly, it was observed that when the gel was photothermally heated, the resistance initially increased then abruptly decreased. The light actuation-recovery shown in Fig. 3e includes following three stages: The step I (0–20 s) involved a rapid volumetric shrinkage and simultaneous resistance increase due to reduced cross-sectional area and internal stress along the restricted axial direction. However, the shrinkage is not sufficient to change the percolation network of PPy. The overall resistivity remained constant and both deswelling and resistance approached a stable point. As NIR illumination continues, the step II (20–26 s) involved a phase change of PPy, which triggered an abrupt further shrinkage (the cliff at 20 s). However, the resistance change was opposite to the predicted geometric effect in the first step. It is proposed by the percolation conduction theory that, above such a threshold density, percolation conduction is enabled by formation of a fully-continuous PPy network [58], rendering the composite significantly more conductive. This resistivity effect subsequently dominated over the geometric effect and resulted in decreased apparent resistance at larger shrinkage volumes. The step III (after 26 s) showed that the sample geometry and resistance recovered to their initial values after the NIR source was switched off at 26 s.

Fig. 4a and b depict the cyclic and reversible changes of resistance under periodic stretching-releasing of c-NanoH samples. The response time was observed to be much less than 1 s, comparable to typical hydrogel strain sensors. To demonstrate the application as a practical sensor, a test was performed where c-NanoH served as an electronic skin affixed to a joint of a human forefinger, and the corresponding variations in resistance upon multi-cycle deformations were observed to be rapid and stable, as seen in Fig. 4c, d, Fig. S3 and Video S2.

The interpenetrating PPy particles play several roles in the composite hydrogel, as pathways for electron transport and

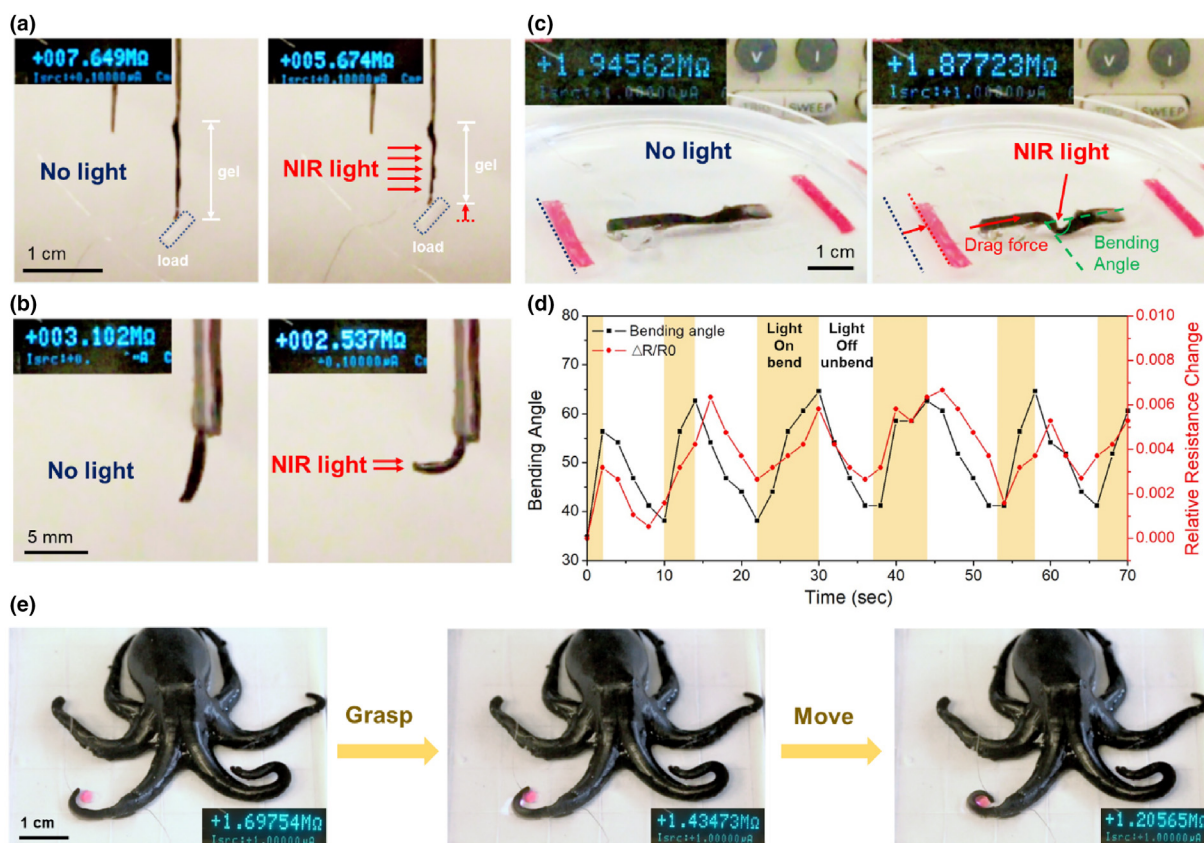


FIGURE 6

(a) Self-sensing weight-lifting in air. (b) Self-sensing “sit-ups” induced by light tracking in air. (c) Stable and completely reversible self-sensing robot in water. (d) The bending angle coincides with the resistance change in the reversible self-sensing robot in water. (e) Self-sensing grasping motion by NIR manipulated local stimulation.

photothermal transducers. Underwater, we measured that the local temperature of hydrogel with PPy increased from 25 °C to as high as 38 °C within 20 s under NIR irradiation. We also demonstrated that increasing PPy concentration, exposure time, and illumination intensity can substantially improve the photothermal effect (Fig. S4). Therefore, besides the function of strain sensing, the composite hydrogels exhibited photo-responsiveness via photo-thermal-mechanical conversion. The composite hydrogels are chemically homogeneous without an observed composition gradient, able to actuate with large flexibility. In addition, we synthesized c-NanoH hydrogel pillars with cylindrical geometry. When NIR light was illuminated on a side of the pillar at an oblique angle, it was able to bend and self-orient towards the light direction. Such directional, asymmetric motion was attributed to temperature gradient across the hydrogel by controlling appropriate light intensity [59]. As depicted in simulation snapshots in Fig. 5, when NIR laser is irradiated on the hydrogel pillar, temperature gradient is generated across the pillar cross-section, in which the temperature on the illuminated side is elevated above the LCST while the temperature on the non-illuminated side remains lower than the LCST; this causes local shrinking solely on the illuminated side, ultimately resulting in precise pillar bending towards the light source.

Furthermore, this self-sensing actuator could perform omnidirectional actuation due to its homogeneous and isotropic structure and local deformation, in contrast to conventional actuators with restricted directionality, anisotropic structure, and uniform deformation. Previously, we have reported isotropic responsive materials that successfully achieved phototropism in response to green and white light based on a negative feedback mechanism [60,61]. In this work, the cylindrical pillar exhibited rapid and omni-directional tracking performance stimulated by NIR light. The tracking capability was demonstrated at an incident light angle of 90°, showing precise control (Fig. 5a). The bending speed reached 34.6°/s. The diffusion time scale was in the range of seconds, which was an order of magnitude faster than the conventional PNIPAAm gels [62]. To further improve the response speed, one can manipulate the hydrogel morphology from closed pore to open pore, leading to enhanced water diffusion rate. [63–65] In addition, the hydrogel pillar could precisely track light sources from different azimuthal angles in the x-y plane, as demonstrated in Fig. 5b. The simulation results showed an excellent match with experimental observation (Fig. 5c, Video S4). Therefore, the fast and omni-directional light-tracking behavior confirms the versatility of this photo-responsive actuator design.

Based on the separately demonstrated strain sensing with a broad actuation range and fast photothermal response, we

further realized combined function of real-time self-sensing actuation. The c-NanoH hydrogel was illuminated with NIR light, causing multiple types of shape change, while an electrical signal across the two terminals of the hydrogel was collected; in this experiment, we were able to accurately monitor shape changes in real-time. Firstly, we mounted and dangled the hydrogel vertically, with electrodes attached to its two ends. The NIR light was illuminated horizontally on the body of the hydrogel. Various photo-actuated motions have been demonstrated, such as uniaxial shrinkage (Fig. 6a, Video S5) with a load attached to the gel bottom and light tracking (Fig. 6b, Video S6) while suspended in air. The hydrogel was strong enough in the air to lift a small weight from uniaxial shrinkage and to perform “sit-ups” from light tracking. During this process, we found that the resistance dropped dramatically during the deformation, due to the percolation-induced conductivity increase associated with the volume shrinking. We also demonstrated that the self-sensing actuation was stable and completely reversible from the submerged cyclic bending experiment, provided there is enough water (Fig. 6c, Video S7). The moving pattern of the bending angle coincided with the resistance change pattern, as shown in Fig. 6d. Furthermore, we showcased c-NanoH's self-sensing ability by remotely controlling a hydrogel octopus arm with NIR light to curl up, grasp, and move an object with real-time motion sensing enabled by monitoring the resistance change between attached electrodes (Fig. 6e, Video S8). The capability of simultaneous self-sensing and actuation provides substantial potential for closed-loop control with no additional external components, helpful for actively predicting and manipulating the motion based on sensing signals. In addition, we anticipate that the future study of the work is going to differentiate the deformation modes for complex robotic application, which can be achieved by incorporation of multiple self-sensing actuators component or embedding multiple pairs of electrodes in one hydrogel.

Conclusions

We presented a self-sensing actuator by in-situ polymerizing a conductive PPy polymer network inside an ultra-stretchable and rapid thermal-responsive nanostructured PNIPAAm hydrogel matrix. The self-monitoring actuator was realized by combining actuation and sensing capabilities into a single composite material. This unique design prevents potential cracking and long-term damage associated with modulus mismatch at the sensor-actuator interface. Precisely controlled local actuation was achieved by NIR laser illumination, where PPy acted as both photothermal transducer and electrical conductor. With a homogeneous structure, the hydrogel could exhibit various omnidirectional and anisotropic locomotions through manipulating the light stimulus. Agile, delicate, and on-demand motions were achieved. The presented composite hydrogel was able to translate the local strain, curvature, bending angle, and surrounding heat into a more visualized quantitative electric signal. Thus, the presented self-sensing, photothermal responsive actuator provides a platform for intrinsic self-monitoring without a need for bulky external equipment, enabling unprecedented closed-loop control of miniature untethered soft robots.

CRedit authorship contribution statement

Chiao-Yueh Lo: Methodology, Writing - original draft. **Yusen Zhao:** Methodology, Validation, Writing - review & editing. **Cheolgyu Kim:** Software. **Yousif Alsaïd:** Writing - review & editing. **Roosbeh Khodambashi:** Methodology. **Matthew Peet:** Resources. **Rebecca Fisher:** Resources. **Hamid Marvi:** Resources. **Spring Berman:** Resources. **Daniel Aukes:** Resources. **Ximin He:** Conceptualization, Methodology, Writing - review & editing, Resources.

Declaration of Competing Interest

The authors declare that they have no known competing financial interests or personal relationships that could have appeared to influence the work reported in this paper.

Acknowledgements

All authors acknowledge ONR awards N000141712117. C. Lo, Y. Zhao, Y. Alsaïd, and X.H. acknowledges N00014-18-1-2314, AFOSR awards FA9550-17-1-0311, FA9550-18-1-0449 and FA9550-20-1-0344, and NSF CAREER award 1724526.

Appendix A. Supplementary data

Supplementary data to this article can be found online at <https://doi.org/10.1016/j.mattod.2021.05.008>.

References

- [1] M.A. McEvoy, N. Correll, *Science* 347 (6228) (2015) 1261689.
- [2] G.-Z. Yang et al., *Sci. Robotics* 3 (14) (2018) eaar7650.
- [3] M. Amjadi, M. Sitti, *Adv. Sci.* 5 (7) (2018) 1800239.
- [4] H.H. Cheng et al., *ACS Nano* 10 (10) (2016) 9529.
- [5] D. Yang et al., *Adv. Mater. Technol.* 1 (3) (2016) 1600055.
- [6] H. Yuk et al., *Nat. Commun.* 8 (2017) 14230.
- [7] C. To et al., Highly stretchable optical sensors for pressure, strain, and curvature measurement, in: *IEEE/RISJ International Conference on Intelligent Robots and Systems (IROS)*, GERMANY, Hamburg, 2015, p. 5898.
- [8] H. Zhao et al., *IEEE Robotics Automation Magazine* 23 (3) (2016) 55.
- [9] H. Zhao et al., *Sci. Rob.* 1 (1) (2016) eaai7529.
- [10] C. Larson et al., *Science* 351 (6277) (2016) 1071.
- [11] X. Yuan et al., Soft tactile sensor and curvature sensor for caterpillar-like soft robot's adaptive motion, in: *Proceedings of the 2019 International Conference on Robotics, Intelligent Control and Artificial Intelligence*, 2019, p. 690.
- [12] F. Spina et al., *Flexible Printed Electronics* 4 (3) (2019) 035001.
- [13] X. Fang et al., A soft actuator with tunable mechanical configurations for object grasping based on sensory feedback, in: *2019 2nd IEEE International Conference on Soft Robotics (RoboSoft)*, IEEE, 2019, p. 25.
- [14] K. Elgeneidy et al., *Mechatronics* 50 (2018) 234.
- [15] R.L. Truby et al., Soft robotic fingers with embedded ionogel sensors and discrete actuation modes for somatosensitive manipulation, in: *2019 2nd IEEE International Conference on Soft Robotics (RoboSoft)*, IEEE, 2019, p. 322.
- [16] R.L. Truby et al., *Adv. Mater.* 30 (15) (2018) 1706383.
- [17] S. Wei et al., *J. Mater. Chem. C* 7 (22) (2019) 6786.
- [18] M.D. Dickey, *Adv. Mater.* 29 (27) (2017) 1606425.
- [19] J.C. Yeo et al., *Adv. Mater. Technol.* 1 (3) (2016) 1600018.
- [20] H. Zeng et al., *Adv. Mater.* 30 (24) (2018) 1703554.
- [21] A. O'Halloran et al., *J. Appl. Phys.* 104 (7) (2008) 9.
- [22] C. Liu et al., *J. Mater. Chem. A* 17 (16) (2007) 1543.
- [23] S.-J. Jeon et al., *Acc. Chem. Res.* 50 (2) (2017) 161.
- [24] L. Chen et al., *Soft Matter* 6 (12) (2010) 2708.
- [25] X.B. Zhang et al., *Nano Lett.* 11 (8) (2011) 3239.
- [26] C. Ma et al., *Adv. Funct. Mater.* 26 (47) (2016) 8670.
- [27] D. Schmaljohann, *Adv. Drug Deliv. Rev.* 58 (15) (2006) 1655.
- [28] S.K. De et al., *J. Microelectromech. Syst.* 11 (5) (2002) 544.
- [29] D. Han et al., *ACS Appl. Mater. Interfaces* 10 (21) (2018) 17512.
- [30] A. Matsumoto et al., *Biomacromolecules* 5 (3) (2004) 1038.
- [31] Y. Qiu, K. Park, *Adv. Drug Deliv. Rev.* 53 (3) (2001) 321.

- [32] K.L. Ang et al., *Mater. Sci. Eng. C-Biomimetic and Supramolecular Systems* 27 (3) (2007) 347.
- [33] Y. Mori et al., *J. Mater. Sci.* 32 (2) (1997) 491.
- [34] L. Zhao et al., *ACS Appl. Mater. Interfaces* 9 (13) (2017) 11866.
- [35] C. Yang, Z. Suo, *Nat. Rev. Mater.* 3 (6) (2018) 125.
- [36] X.D. Wu et al., *Adv. Funct. Mater.* 26 (34) (2016) 6246.
- [37] J.H. Zhao et al., *Compos. Part A-Appl. Sci. Manuf.* 48 (2013) 129.
- [38] H. Liu et al., *J. Mater. Chem. C* 4 (1) (2016) 157.
- [39] S. Ryu et al., *ACS Nano* 9 (6) (2015) 5929.
- [40] Z. Lei, P. Wu, *Nat. Commun.* 10 (1) (2019) 1.
- [41] C. Cochrane et al., *Sensors* 7 (4) (2007) 473.
- [42] T. Yamada et al., *Nat. Nanotechnol.* 6 (5) (2011) 296.
- [43] N. Hu et al., *Carbon* 48 (3) (2010) 680.
- [44] Y. Shi et al., *Adv. Funct. Mater.* 25 (8) (2015) 1219.
- [45] K. Wang et al., *Adv. Mater.* 27 (45) (2015) 7451.
- [46] M.C. Koetting et al., *Mater. Sci. Eng.: R: Rep.* 93 (2015) 1.
- [47] W. Jayathilaka et al., *Adv. Mater.* 31 (2019) 7.
- [48] P.T. Lai et al., *IEEE Electron Device Lett.* 20 (11) (1999) 589.
- [49] J.P. Bentley, *J. Phys. E-Sci. Instruments* 17 (6) (1984) 430.
- [50] J. Harreld et al., *J. Non-Cryst. Solids* 225 (1) (1998) 319.
- [51] Y. Guo et al., *Small* 14 (14) (2018) 1704497.
- [52] K. Sun et al., *ACS Sustainable Chem. Eng.* 7 (1) (2018) 165.
- [53] N.V. Blinova et al., *Eur. Polym. J.* 43 (6) (2007) 2331.
- [54] H. Yamauchi, Y. Maeda, *J. Phys. Chem. B* 111 (45) (2007) 12964.
- [55] L.-W. Xia et al., *Nat. Commun.* 4 (1) (2013) 1.
- [56] Y.Y. Lee et al., *Adv. Mater.* 28 (8) (2016) 1636.
- [57] Y. Wang et al., *Sci. Adv.* 3 (3) (2017) e1602076.
- [58] H. Liu et al., *J. Mater. Chem. C* 6 (45) (2018) 12121.
- [59] X. Qian et al., *Nat. Nanotechnol.* (2019) 1.
- [60] X.M. He et al., *Nature* 487 (7406) (2012) 214.
- [61] Y. Zhao et al., *Sci. Rob.* 4 (33) (2019) eaax7112.
- [62] E.S. Gil et al., *Langmuir* 26 (19) (2010) 15614.
- [63] R. Khodambashi et al., *Adv. Mater.* (2021) 2005906.
- [64] Y. Alsaied et al., *Adv. Mater.* (2021) 201701938.
- [65] S. Wu et al., *EcoMat* (2021) 1.